Energy 113 (2016) 432–443

Contents lists available at ScienceDirect

Energy

journal homepage: www.elsevier.com/locate/energy

Controlled deposition and utilization of carbon on Ni-YSZ anodes of SOFCs operating on dry methane

Yong Jiao [a], Liqin Zhang [a], Wenting An [a], Wei Zhou [b], Yujing Sha [b], Zongping Shao [b, c, *], Jianping Bai [d], Si-Dian Li [a]

[a] Key Laboratory of Materials for Energy Conversion and Storage of Shanxi Province, Institute of Molecular Science, Shanxi University, No. 92 Wucheng Road, Taiyuan 030006, PR China
[b] State Key Laboratory of Materials-Oriented Chemical Engineering, College of Chemistry & Chemical Engineering, Nanjing Tech University, No. 5 Xin Mofan Road, Nanjing 210009, PR China
[c] College of Energy, Nanjing Tech University, No. 5 Xin Mofan Road, Nanjing 210009, PR China
[d] State Energy Key Laboratory of Coal and Coalbed Methane Co-mining, Shanxi Lanyan Coalbed Methane Group Co., Ltd, No. 797 Lanhua Road, Jincheng 048000, PR China

ARTICLE INFO

Article history:
Received 11 April 2016
Received in revised form
11 July 2016
Accepted 12 July 2016
Available online 22 July 2016

Keywords:
Solid oxide fuel cell
Nickel-based anodes
Operating stability
Controlled carbon deposition
Methane supply mode

ABSTRACT

Solid oxide fuel cells (SOFCs) are promising power-generation systems to utilize methane or methane-based fuels with a high energy efficiency and low environmental impact. A successive multi-stage process is performed to explore the operation of cells using dry methane or the deposited carbon from methane decomposition as fuel. Stable operation can be maintained by optimizing the fuel supply and current density parameters. An electrochemical impedance analysis suggests that the partial oxidization of Ni can occur at anodes when the carbon fuel is consumed. The stability of cells operated on pure methane is investigated in three operating modes. The cell can run in a comparatively stable state with continuous power output in an intermittent methane supply mode, where the deposition and utilization of carbon is controlled by balancing the fuel supply and consumption. The increase in the polarization resistance of the cell might originate from the small amount of NiO and residual carbon at the anode, which can be removed via an oxidation-and-reduction maintenance process. Based on the above strategy, this work provides an alternative operating mode to improve the stability of direct methane SOFCs and demonstrates the feasibility of its application.

1. Introduction

In the last decades, fuel cells have received growing attention as one of the major types of sustainable energy, and have been advocated as a more efficient and cleaner energy alternative [1–5]. SOFCs (solid oxide fuel cells) are all-solid-state energy conversion devices that typically operate at approximately 600–1000 °C with great fuel flexibility [6–9]. Recently, methane-based fuels, including natural gas, shale gas, coalbed gas and biogas, have increasingly become the preferred fuel choice for SOFCs due to their wide availability [6,7]. SOFCs operating directly on methane or methane-based fuels could be more cost-effective owing to their high overall fuel efficiency and system simplicity [7].

Nickel cermets are the most commonly used anode materials for SOFCs, and they show superior performance in terms of activity towards hydrogen electrocatalytic oxidation, electronic conductivity, and thermo-mechanical compatibility with electrolytes [6]. In addition, nickel cermets have been proven to be feasible in processing and cost, especially in anode-supported SOFCs [7]. However, a major challenge is that the nickel-based anodes tend to cause carbon deposition from methane fuel [10–12]. Nickel catalyzes the methane decomposition reaction (Eq. (1)), resulting in coke formation and the deactivation of the anode [12].

$$CH_4 \rightarrow C + 2H_2 \quad (1)$$

There has been considerable literature on modifying of Ni-based anodes or developing alternative anode materials to avoid carbon deposition [13–17]. Steady operation of SOFCs with hydrocarbon fuels has been demonstrated by applying ceria as an interlayer

* Corresponding author. State Key Laboratory of Materials-Oriented Chemical Engineering, College of Chemistry & Chemical Engineering, Nanjing Tech University, No. 5 Xin Mofan Road, Nanjing 210009, PR China.
E-mail address: shaozp@njtech.edu.cn (Z. Shao).

http://dx.doi.org/10.1016/j.energy.2016.07.063
0360-5442/

between the YSZ electrolyte and the Ni-YSZ anode [13] or as a component of Cu-based anodes [14]. While many alternative anode materials can be operated on hydrocarbon fuels without carbon deposition, the performance of the corresponding SOFCs cannot compare with that of Ni-YSZ anode SOFCs [12]. Therefore, utilizing the heavily developed Ni-YSZ anodes is desirable.

The activity of SOFC anodes is well known to be dependent not only on materials but also on the microstructure and operating conditions [7,18,19]. Optimizing the operating conditions can both promote electrochemical methane oxidation and inhibit carbon deposition. Current density is one of the crucial operating parameters to suppress carbon deposition on anodes. Koh et al. [12] reported that the chemical equilibrium behaviors of methane on SOFC anodes can be explained by three overall methane reactions. Carbon is significantly deposited at the open circuit condition (Eq. (1)) and is rapidly reduced as current is applied to the cell (Eq. (2)). Equation (3) is considered dominant at current densities much higher than the critical current density (Jc), above which no carbon deposition is observed.

$$CH_4 + O^{2-} \rightarrow CO + 2H_2 + 2e^- \quad (2)$$

$$CH_4 + 4O^{2-} \rightarrow CO_2 + 2H_2O + 8e^- \quad (3)$$

Alzate-Restrepo et al. [20] reported that the amount of deposited carbon on Ni–YSZ anodes exposed to methane decreased as the current density increased. Lin et al. [10] studied the stability of cells operated on methane at different current densities and temperatures and indicated that the O^{2-} flux through the SOFC was at least partly responsible for preventing coking and for thereby maintaining stable operation. Liu et al. [21] reported that Ni-YSZ anode SOFCs could be stably operated on humidified methane for >90 h at 700 °C, suggesting that carbon deposition was limited under high current densities.

An increasing body of evidence suggests that carbon deposited on Ni-YSZ anodes can be oxidized electrochemically (Eqs. (4) and (5)) [22–25].

$$C + O^{2-} \rightarrow CO + 2e^- \quad (4)$$

$$C + 2O^{2-} \rightarrow CO_2 + 4e^- \quad (5)$$

The O^{2-} in the anode ionic conductor is promoted by the polarization current to react with carbon and release electrons into the external circuit. The carbon deposited at the TPB and the YSZ and Ni particle surfaces can all participate in the electrochemical reactions [23]. Carbon at the YSZ is likely to react with the O^{2-} conducted through the YSZ, and electrons are conducted through the Ni and deposited carbon with good electronic conductivity. It was reported that the O^{2-} conducted through the YSZ can spill over from the polarized Ni–YSZ interface onto the Ni surface [26,27]. Then, the supplied O^{2-} can effectively react with the carbon on the Ni, which might be eliminated if the amounts of O^{2-} were appropriately controlled. Ihara et al. [28–31] developed a rechargeable direct carbon fuel cell (RDCFC) using the deposited carbon from the decomposition of methane or propane at the anode under OCV (open circuit voltage) as the fuel. The operation of RDCFCs with Ni-GDC anodes was highly stable after six cycles of carbon deposition and power generation.

In the present work, the controlled deposition and utilization of carbon on Ni-YSZ anodes of SOFCs operating on dry methane was studied. The carbon deposition was controlled to be as reversible as possible by optimizing the cell operating parameters, and the limited carbon deposition was used as fuel for SOFCs. The cell's stability was significantly improved with continuous power output under a cycling mode with an intermittent supply of pure methane. Under this mode, the deposition and utilization of carbon was well controlled by balancing the fuel supply and consumption.

2. Experimental

2.1. Cell fabrication

Anode-supported cells with yttria-stabilized zirconia (YSZ) thin-film electrolyte were fabricated using a modified procedure from the literature [32]. NiO (Chengdu Shudu Nanomaterials Technology Development Co. Ltd., China) and YSZ (Tosoh Corporation, Japan) at a weight ratio of 3:2 were mixed in ethanol by high-energy ball milling (Fritsch Pulverisettle 6, Fritsch GmbH, Idar-Oberstein, Germany) at a rotation rate of 400 rpm for 0.5 h, and 7 wt% (relative to the NiO+YSZ) of polyvinyl butyral (PVB) was added and dispersed in the mixture by magnetic stirring for 2 h, which was subsequently dried and ground with a mortar and pestle then passed through a 150 μm mesh sieve. The mixed anode powder was first pressed as a substrate in a stainless steel die, then pure YSZ powder was added onto the substrate and co-pressed to form a bi-layer pellet. The electrolyte thickness was controlled by the amount of YSZ applied. The green pellets were then sintered in air at 1400 °C for 5 h to densify of the electrolyte layer.

A Sr-doped $LaMnO_3$ powder was prepared by a sol–gel technique reported elsewhere [33]. To prepare the cathode, the homemade $La_{0.8}Sr_{0.2}MnO_3$ (LSM) powder was first prepared into a colloidal suspension by dispersing it into a mixed solution of glycerol, ethylene glycol and isopropyl alcohol by high-energy ball milling. The colloidal suspension was then sprayed under the drive of 1 atm nitrogen carrier gas onto the central surface of the electrolyte using a modified spraying gun (BD-128, Fenghua Bida Machinery Manufacture Co. Ltd., China) with a nozzle size of 0.35 mm (pore diameter). The spray gun was aligned above the heated substrate (250 °C on a hot plate) at a distance of approximately 10 mm. The cells were then sintered at 1100 °C for 2 h in stagnant air. The cathode effective area was approximately 0.48 cm^2. Silver was adopted as the current collector for both electrodes. The typical cell microstructure is shown in Fig. 1(b).

2.2. Test setup

The single cell test setup is shown schematically in Fig. 1(a). The cell was sealed onto the quartz tube using silver paste with the cathode exposed to ambient air. Voltage versus current density polarization curves were obtained using a four-terminal configuration to eliminate the ohmic loss in the silver wires. Electrochemical impedance spectra (EIS) were measured under open-circuit conditions with a frequency range from 0.1 Hz to 100 kHz and an alternate current signal amplitude of 10 mV. Electrochemical data were collected using an Iviumstat electrochemical analyzer (Ivium Technologies B.V., Netherlands). A JEOL JEM-2100 scanning electron microscope (SEM) was employed to examine of the anode microstructure. The cross-sectional morphology of the fuel cell was examined using an environmental scanning electron microscope (ESEM, FEI, Quanta-200).

2.3. Testing procedure

In general, the anode was first reduced in H_2 with a flow rate of 40 ml min^{-1} at 700 °C for 1 h, and was then purged by Ar with a flow rate of 100 ml min^{-1} for at least 30 min. After gradually increasing the temperature to the target value, the fuel supply was switched to a certain fuel composition and the cell performance was measured.

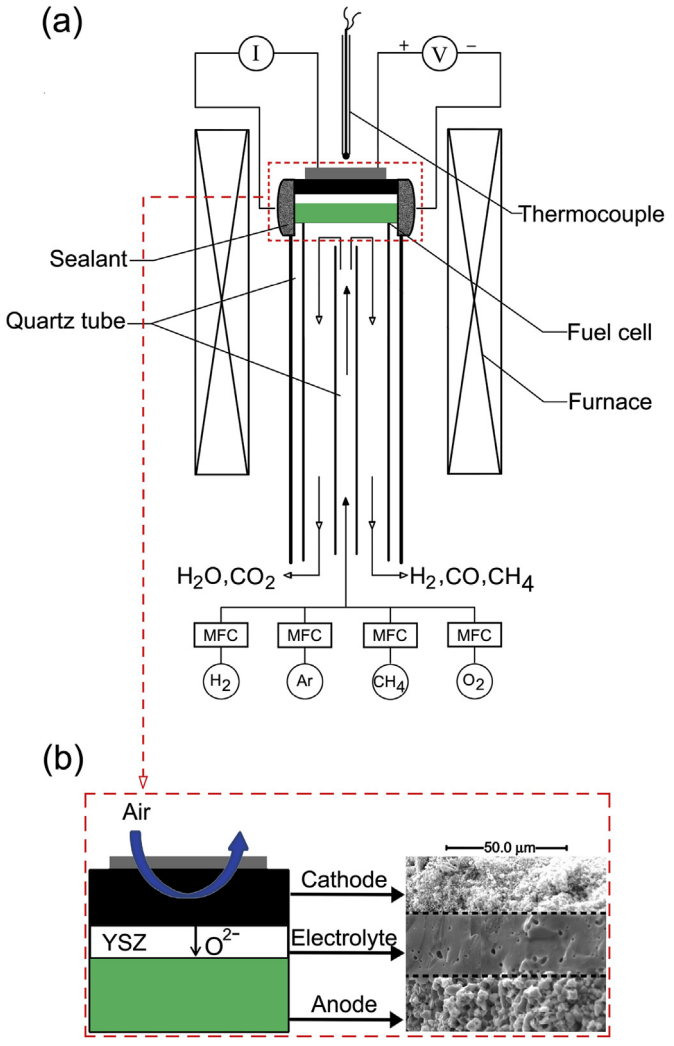

Fig. 1. (a) Schematic of the fuel cell test setup, and (b) the schematic structure (left) and a typical SEM image of the SOFC microstructure (right).

The procedures in Fig. 2(a), Fig. 2(b) and (c) are related to the experiments in Fig. 4(a), Fig. 8 and Fig. 9(a), respectively. Fig. 2(a) shows the procedure of a successive seven-stage process performed to examine carbon deposition on the anode of cells operated on dry methane, and to examine whether the deposited carbon can be used as fuel for the cell. Stage I is a normal H_2 reduction of anodes with a flow rate of 40 ml min^{-1} at 700 °C for 1 h. The anode was then purged by Ar with a flow rate of 100 ml min^{-1} for at least 30 min in Stage II. In Stage III, the fuel supply is switched to 25% dry methane in Ar at 40 ml min^{-1} under open circuit conditions. The cell is then operated on this fuel composition for 2 h at 625 mA cm^{-2} at 800 °C in Stage IV. Stage V is another purging process to remove CH_4. In Stage VI, the cell is operated with the deposited carbon at a constant current density under the protection of Ar. Stage VII is a step to reduce the partially oxidized anode. Fig. 2(b) shows the RDCFC cycling operation procedure performed to examine the feasibility of cells running under the RDCFC mode at selected conditions. The RDCFC mode generally consists of several cycles and each cycle includes two stages, i.e., the charging and discharging stages [28–30]. In the so-called charging stage, the carbon fuel is loaded on the anode by depositing carbon from the thermal decomposition of hydrocarbons (methane, propane, etc.) under the OCV state. In the discharging stage, electric power is generated using the pyrolytic carbon as fuel. In the present work, the charging stage was performed by feeding 80 ml min^{-1} pure methane for 4.5 min at 825 °C. Then, the discharging stage was started at 416 mA cm^{-2} and lasted approximately 7 min until the voltage dropped to zero. Fig. 2(c) shows the cycling operation procedure performed to demonstrate the intermittent fuel supplying mode (IFS), a novel operating mode for controlled carbon deposition and utilization of the cell directly using dry methane, where the cell was also operated in a two-stage cycle: a methane supply stage and a period of stopping the methane supply. In the former stage, the cell was operated at 416 mA cm^{-2} for 5 min under the same flow rate of methane and temperature as the RDCFC mode. In the later stage, the cell was operated at 416 mA cm^{-2} by using the deposited carbon as fuel. The former stage would re-start once the voltage dropped to approximately 0.7 V.

3. Results and discussion

3.1. Current-voltage benchmark measurements

The object of the benchmark tests was to check the reliability of SOFCs used in this work. Fig. 3(a) shows the typical I-V and I-P characteristics of an SOFC operating on hydrogen at different temperatures. The OCV values for hydrogen reached 1.153, 1.144, and 1.123 V at 750, 800, and 850 °C, respectively, which indicate that the electrolyte film was sufficiently dense to prevent the crossover of the gases and that the cell was sealed tightly. The decrease in the OCV values for hydrogen with the increasing temperature is consistent with prior results and theoretical expectations [10,12]. The root reason for this phenomenon is that the share of heat energy among the total energy released by the cell reaction increases with the increasing temperature, while the share of energy converting into electrical energy reduces [34,35]. All of the I-V curves were clearly non-linear to some extent in Fig. 3(a). The activation polarization at low current density for hydrogen became more apparent with the decrease in the operating temperature.

Fig. 3(b) compares the electrochemical performance of methane with hydrogen at 825 °C. The OCV for methane is 1.221 V and 1.136 V for hydrogen. The peak power density (PPD) for methane is 680 mW cm^{-2}, which is 9.3% lower than that for hydrogen, 750 mW cm^{-2}. The activation polarization at low current density for methane is higher than that for hydrogen, suggesting that the electrochemical oxidation step is slower for methane. In addition, the concentration polarization for methane is also higher than that for hydrogen at high current density. This may due to the higher molecule mass of methane than that of hydrogen, which yields slower gas phase diffusion. All the above results agree well with prior reports [10,11].

3.2. A typical dissecting process to examine carbon deposition and availability thereof

The aim of the experiments related to Fig. 4 was to examine carbon deposition on the anode of SOFCs operating on dry methane and to demonstrate the availability of deposited carbon as a fuel for SOFCs under the DCFC (direct carbon fuel cell) mode [22–25]. Fig. 4(a) shows the seven-stage experiment performed successively by operating the cell on switching the fuel from hydrogen, dry methane to deposited carbon (see Fig. 2(a) for procedures). The cell's electrochemical behavior at the boundary points where the fuel type was switched was tested (see Fig. 4(b)-(e)). These boundary points were termed as the monitoring points (MP) herein.

Selection of the key operating parameters: current density and temperature. Several researchers have demonstrated that the O^{2-} flux through SOFCs can significantly suppress carbon deposition

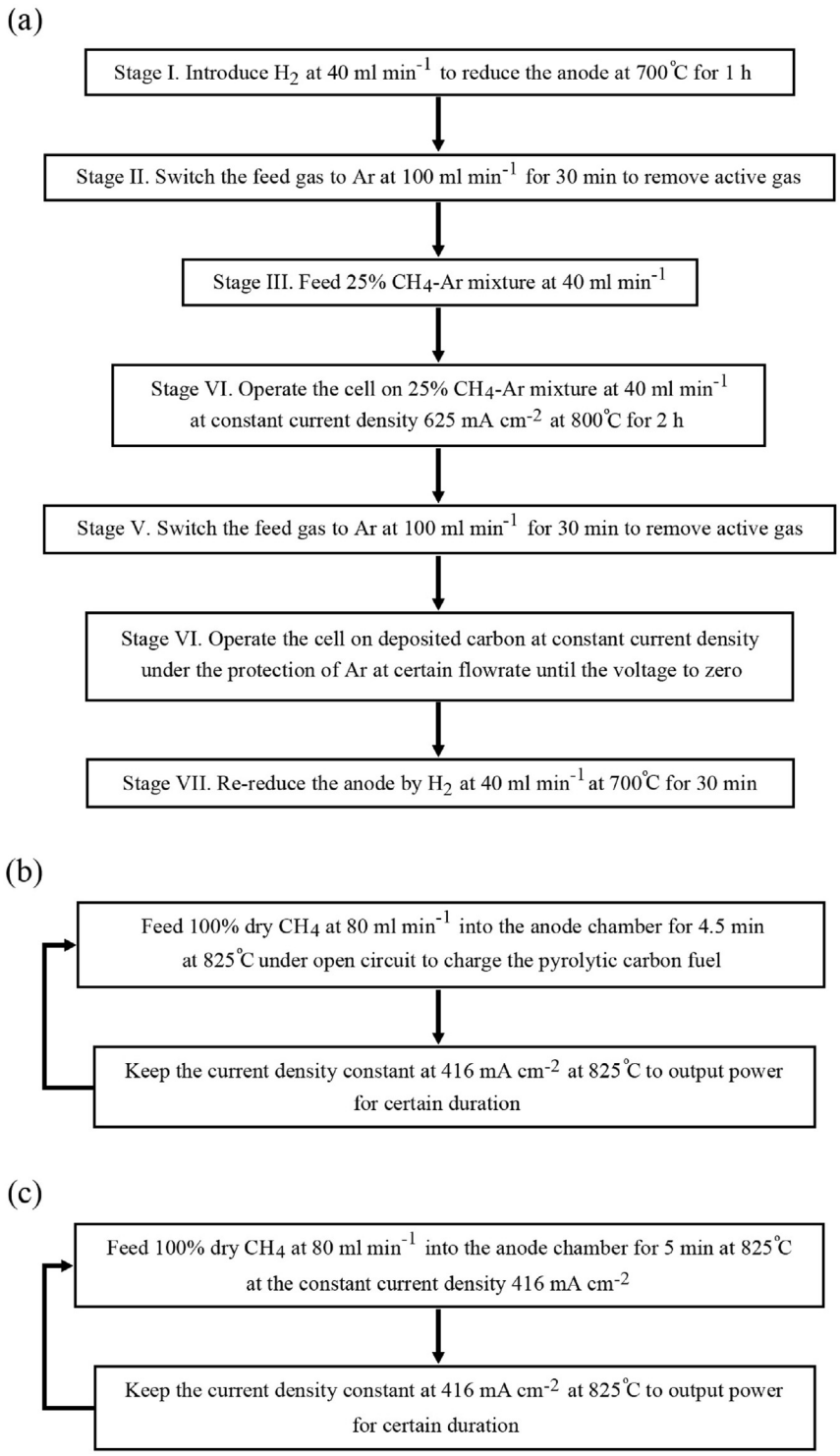

Fig. 2. Flow charts of the procedures in (a) the successive multi-stage process, (b) the rechargeable direct carbon fuel cells (RDCFC) process, and (c) the intermittent fuel supply mode.

and maintain the stable operation of the cell [7]. With the increasing O^{2-} flux from the cathode to the anode, the conversion of methane over the anode into CO, H_2, CO_2, and H_2O has been shown to increase, and the amount of carbon deposition from methane decomposition is rapidly decreased. In particular, when the loaded current density was above the critical current density (J_c), the carbon deposition could almost be neglected [12].

To suppress carbon deposition in SOFCs using methane fuel, the following two points were considered to determine the key operating parameter, that is, the constant working current density J_w: (i) to maintain the cell's power output as close to its PPD as possible; (ii) to maintain the terminal voltage as stable and relatively high. Thus, $J_w = 625$ mA cm^{-2} was chosen based on the I-V curves in Fig. 4(b) and was applied at stage IV in Fig. 4(a) when the fuel was switched to dry methane. As seen in Fig. 4(a), at this J_w, the cell was operated near its PPD, and the terminal voltage was maintained basically as stable.

The operating temperatures ≧800 °C were selected herein

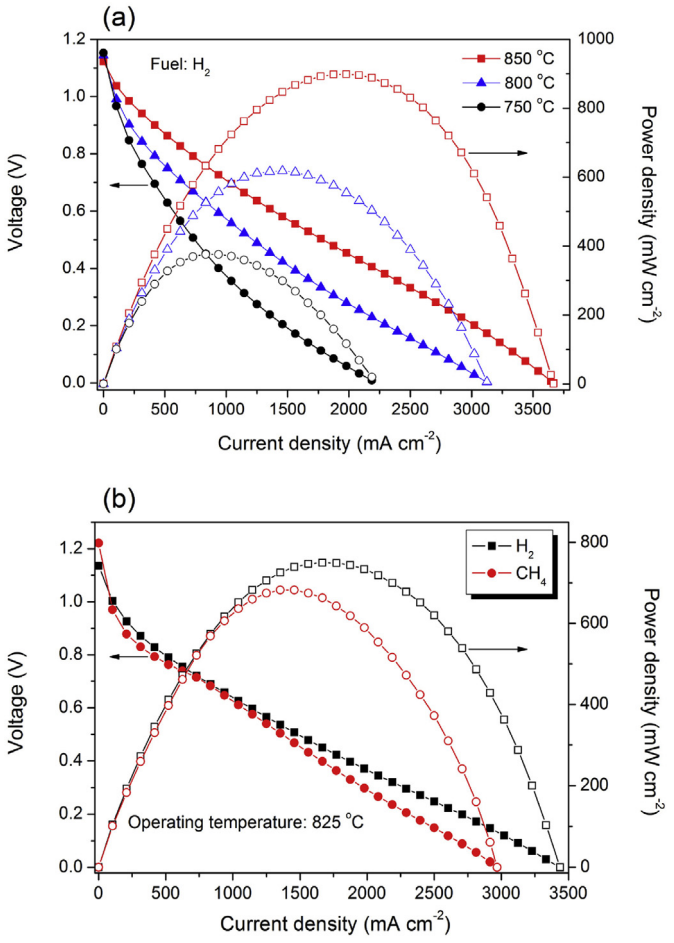

Fig. 3. I-V and I-P curves of the cells operated (a) on H_2 at various temperatures, and (b) on H_2 and CH_4 at 825 °C. The flow rate of each gas was 40 ml min^{-1}.

based on the following main considerations: (i) the methane decomposition reaction (Eq. (1)) is moderately endothermic (ΔH^0_{298} = 74.8 kJ mol^{-1}), which is kinetically unfavorable at temperatures below 700 °C. To accelerate the carbon deposition process, temperatures >700 °C are generally considered; (ii) the LSM cathode typically works at high temperature (800–1000 °C), and the overpotential increases significantly below 800 °C due to the relative low reaction rate of oxygen reduction [36]. Alternative cathode materials must be considered for high electrochemical performance below 800 °C.

Stability of the cell operated on dry methane. Stage IV in Fig. 4(a) shows the stability test of the cell operated on 25% dry methane in Ar at 800 °C. At J_w = 625 mA cm^{-2}, the cell operation was moderately stable with an average power density of approximately 394 mW cm^{-2} over the 120 min test period, which is approximately the value expected by the I-V curve measured at monitoring point MP2 in Fig. 4(b). Note that the voltage fluctuated approximately 0.63 V and exhibited a slight decrease during stage IV.

Ni-based anode SOFCs have been shown to be able to operate stably using humidified methane at relatively high current densities at temperatures <700 °C or at higher temperatures if a substantial cell current density is maintained [10]. The coke-free stable operation has been explained by the relatively low rate of methane cracking at temperatures <700 °C and by the effects of current density and cell reaction products at higher temperature [11].

The I-V curves measured at points MP2 and MP3 in Fig. 4(b) almost overlap each other above 0.4 V, which provides more evidence supporting the high stability. However, as shown in Fig. 4(c), the corresponding electrochemical impedance spectra (EIS) give some different, more detailed information. The impedance spectra measured at points MP2 and MP3 nearly overlap each other except for the bifurcation at low frequency below 10 Hz, which indicates that the polarization resistance increased after stage IV [37–40]. Generally, EIS responses in low frequency (LF≦100 Hz) could be associated with non-charge-transfer processes including gas diffusion [37]. Barnett et al. reported that the responses at 0.5–10 Hz appeared to track with the anode pore connectivity, suggesting they were related to gas diffusion [38]. Herein, the bifurcated responses at ≦10 Hz measured at points MP2 and MP3 suggest that there might be some carbon deposited at the anode during stage IV, which may block the anode pores or reduce the pore connectivity and thus hinder methane diffusing, resulting in the increase of polarization resistance [39]. The lowered anode pore connectivity reduces the active pore volume fraction ε and also increases tortuosity τ, decreasing the effective gas diffusion coefficient D_{eff} given by the equation [40]:

$$D_{eff} = \frac{\varepsilon \cdot D}{\tau^2} \quad (6)$$

Stability of the cell operated on deposited carbon. Stage VI in Fig. 4(a) shows the stability test of the cell operated on deposited carbon in stage IV with J_w = 41.7 mA cm^{-2} under 5 ml min^{-1} Ar protection at 800 °C. The aim of stage VI was to use the deposited carbon as fuel or to remove it by operating the cell in a DCFC (direct carbon fuel cell) mode. The stage lasted approximately 30 min with the voltage gradually decreasing until finally dropping to zero.

Li et al. [23] proposed a detailed mechanism to describe the direct electrochemical reactions of CH_4-deposited carbon on the SOFC anode (see Eq.(12)–(17) below in section 3.4). During the cell discharging, the O^{2-} fluxes from the ionic conductor contact the carbon reactive sites, and the released electrons are conducted to the external circuit. The electrochemical reactivity for the deposited carbon is highly dependent on the deposition sites (or local microenvironment) on the anode, and the reactions are most difficult on the Ni particle surfaces, easier on the YSZ particle surfaces, and easiest at the TPB. In addition, some of the deposited carbon does not participate in the direct electrochemical reactions and becomes residual carbon.

Redox stability of the cell operated on deposited carbon. Fig. 4(d) shows the EIS of the cells using hydrogen as fuel at the points MP1 and MP4 (see Fig. 4(a)) and that of the anode in the full oxidation state. MP1 represents the cell state where the anode was fully reduced, and MP4 represents the state where the DCFC stage just terminated. As shown in the inserted table in Fig. 4(d), the resistance values of MP1, MP4, and the oxidation state at 100 kHz are 0.193, 2.523, and 22.090 Ω cm^2, respectively. The value of the oxidation state is two orders of magnitude higher than that of MP1, showing the large gap in the ohmic resistance between the two extreme redox states of the anode, that is, the fully oxidized state and the fully reduced state at MP1. The value of MP4 is more than ten times higher than that of MP1, yet almost nine times less than that of the oxidation state. Obviously, the anode at MP4 was under a partial oxidation state. Thus, the significant performance degradation at MP4 (Fig. 4(e)) could be attributed to the partial oxidization of Ni in the anode to NiO. Koh et al. [12] reported that the oxidation of Ni predominantly brings about an increase in the ohmic resistance, and the ohmic resistance increases further as the cell is exposed to the oxidative condition longer. Chen et al. [41] reported that the increase in the ohmic resistance of the cell tested at a low hydrogen concentration and high current density indicated that some new materials such as NiO with low electronic

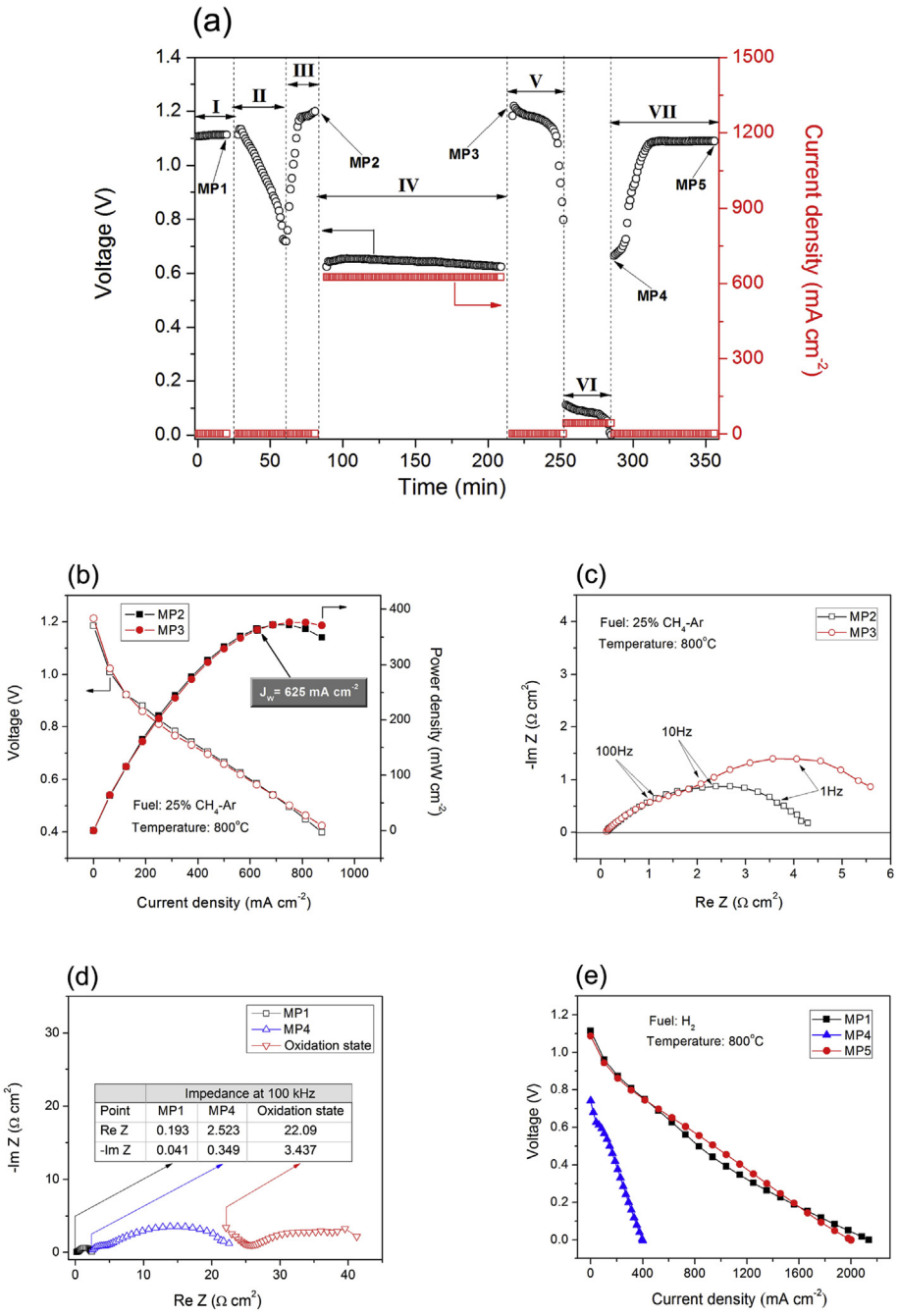

Fig. 4. (a) A successive seven-stage process of an SOFC operated on dry methane and/or deposited carbon at 800 °C. (b) I-V and I-P curves and (c) the impedance spectra of the cells operated on 25% CH_4-Ar at MP2 and MP3. (d) Impedance spectra of the cells operated on H_2 at MP1, MP4 and the oxidation state, and (e) the I-V curves at MP1, MP4 and MP5.

conductivity could be formed after the test.

The cell was reduced again using 40 ml min^{-1} hydrogen in stage VII (Fig. 4(a)), and the OCV increased rapidly to 1.09 V after 30 min reduction, and subsequently maintained this level. Fig. 4(e) shows that the I-V curve measured at MP5 is basically the same as that of MP1, and the OCV values at MP1 and MP5 have almost no change, which reflect that the cell not only maintained its mechanical integrity well but also regained its electrochemical performance after re-reduction.

In brief, the results in Fig. 4 indicate that: (i) The cell could basically run stably at high current density, however, some deposited carbon may still occur at the anode. (ii) The deposited carbon can be used as fuel. (iii) The consumption of deposited carbon could result in the partial oxidation of the anode, yet which can be recovered by hydrogen reduction. The above results suggest that the key stages IV and VI, combining with stage VII, could form a cycle to maintain the cell continuously running (see Fig. 5(a)), which lays a foundation for the multi-cycle operation under the intermittent methane supply mode (see Fig. 5(b)).

Influence of operation parameters on the DCFC mode. Fig. 6 shows the influence of operating variables, i.e., the Ar flow rate and the current density, on the stability of the DCFC mode using CH_4-deposited carbon as fuel. In Fig. 6(a), under $J_w = 10.4$ mA cm^{-2}, with the increase in Ar flow rates from 5 to 10 and 50 ml min^{-1}, the discharging time mildly decrease from 264.0 to 255.4 and 231.9 min, respectively. The data indicate that at the same current

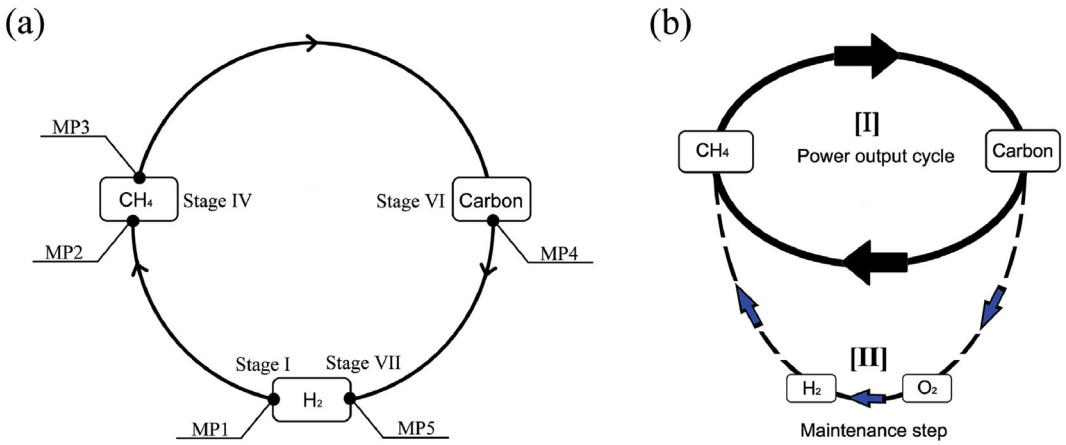

Fig. 5. (a) A cycle based on the experiment in Fig. 4(a). (b) A multi-cycle operation with an oxidation-and-reduction maintenance step under the intermittent methane supply mode (see Section 3.3.3 for detailed description).

density, the lower Ar flow rate resulted in better cell operating stability, although the influence was limited. Ihara et al. [28–31] studied the dependence of power generation of a RDCFC on Ar flow rates and found that there was an optimum value for maximum capacity of power generation. Decreasing the Ar flow rates caused an increase in the partial pressure of CO, which was generated by Boudouard corrosion. The deposited carbon on surfaces other than the TPB could be utilized as a fuel due to the occurrence of Boudouard corrosion. On the other hand, as seen in Fig. 6(b), under the same Ar flow rate of 5 ml min^{-1}, with the increase in J_w from 10.4 to 20.8 and 41.7 mA cm^{-2}, the discharging time rapidly decreased from 264.0 to 106.0 and 31.0 min, respectively. The comparison of different operating variables on the performance of DCFC mode are summarized in Table 1. These results suggest that at the same Ar flow rate, the lower current density results in better cell stability, and the influence of the current density on the operating stability is more significant than that of Ar flow rate.

3.3. Cycling operation mode for controlled deposition and utilization of carbon

3.3.1. Stability test of the cell operated on pure methane by continuous fuel supply mode

As shown in Fig. 7(a), the fuel cell maintained approximately 18 min stable operation using 80 ml min^{-1} pure methane fuel at $J_w = 416$ mA cm^{-2} at 825 °C. During the 18 min period, the voltage fluctuated slightly between 0.75 and 0.8 V and the power density between 313 and 333 mW cm^{-2}. After the 18th minute, the voltage decreased rapidly to zero at 21 min due to a mechanical crack in the cell, which arose from the severe carbon deposition at the anode (Fig. 7(b)). The above results provide very important information for determining the appropriate carbon deposition duration, within which the amount of deposited carbon is small enough to avoid the destruction of fuel cells.

It is well known that a series of reactions may occur once methane reaches the Ni-YSZ anode [7]. The main overall reactions include methane decomposition (Eq. (1)), partial methane oxidation (Eq. (2)), and complete methane oxidation (Eq. (3)). The reforming reactions of methane and carbon are as follows:

$$CH_4 + H_2O \rightarrow CO + 3H_2 \quad (7)$$

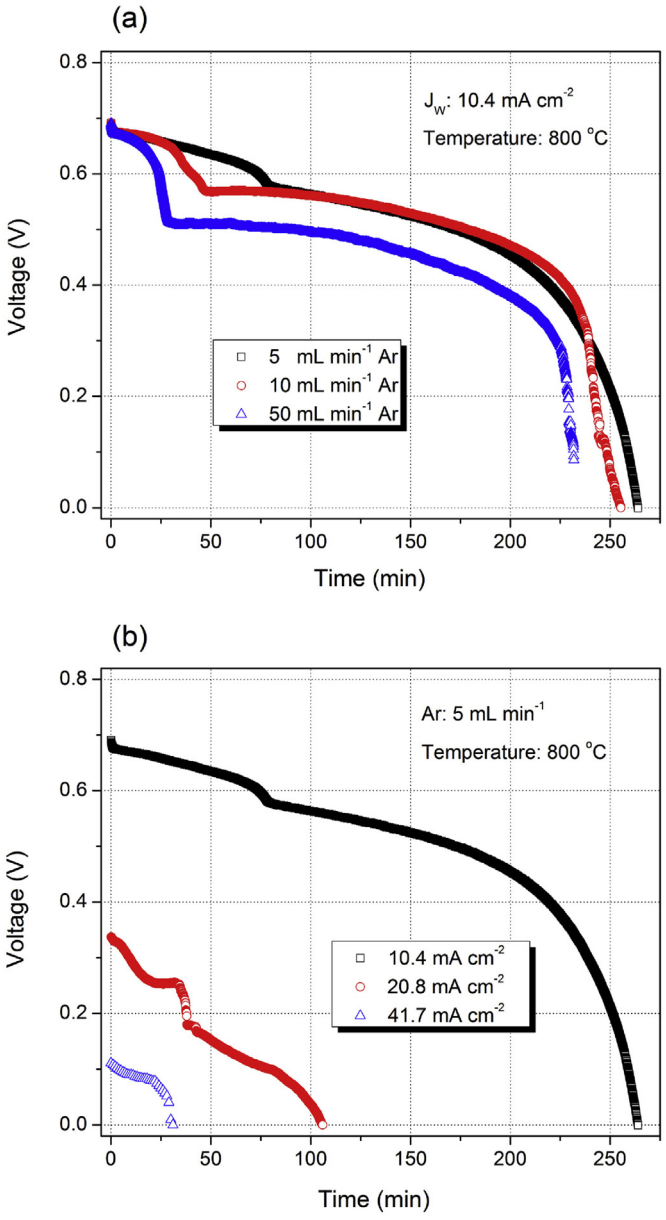

Fig. 6. The influence of (a) Ar flow rates and (b) current densities on the stability of DCFC mode.

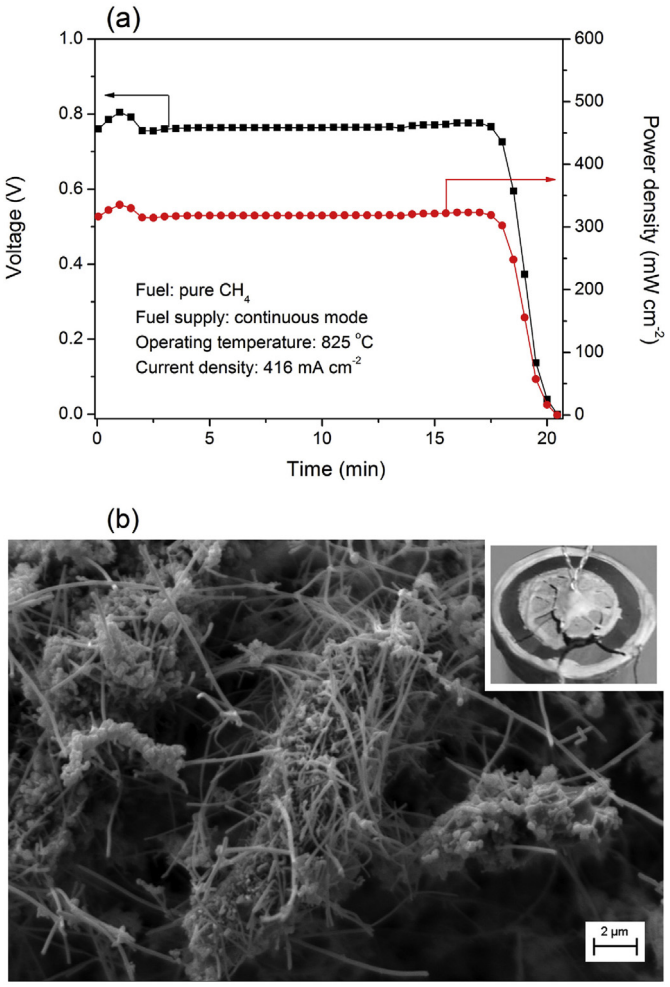

Fig. 7. (a) Voltage (and power density) versus time for the cell operated under the continuous methane supply mode. (b) SEM image of the anode with severe deposited carbon and electronic photo of the cracked cell (the inset at bottom-left) after the continuous fuel supply mode test.

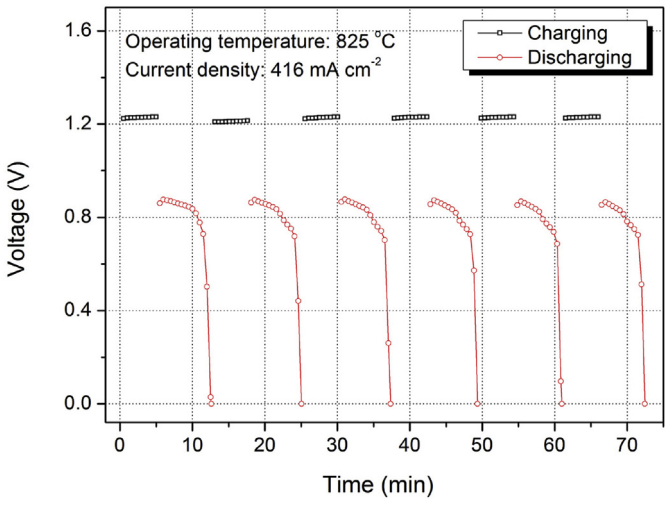

Fig. 8. Voltage versus time for the cell operated under the RDCFC mode.

$$CH_4 + CO_2 \rightarrow 2CO + 2H_2 \quad (8)$$

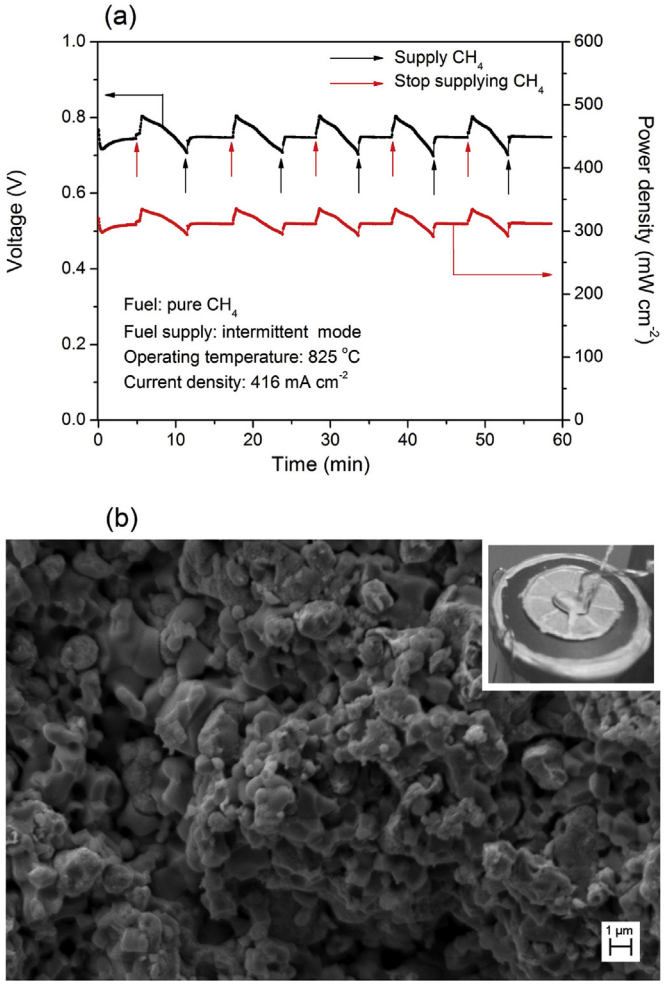

Fig. 9. (a) Voltage (and power density) versus time for the cell operated under the intermittent methane supply mode. (b) SEM image of the anode and photo of the cell (the inset at bottom-left) after the intermittent fuel supply mode test.

Table 1
Comparison of different operating variables on the output of DCFC mode.

Current density (mA cm^{-2})	10.4			20.8	41.7
Ar flow rate (ml min^{-1})	5	10	50	5	5
Charging duration (min)	264.0	255.4	231.9	106.0	31.0
Charging quantity (C)	79.07	76.50	69.46	63.50	37.23
Carbon consumption (g)	0.00246	0.00238	0.00216	0.00197	0.00116

$$C + H_2O \leftrightarrow CO + H_2 \quad (9)$$

$$C + CO_2 \leftrightarrow 2CO \quad (10)$$

When other conditions have been determined, the amount of feed methane and the oxygen ion supply will determine the equilibrium of the complex system at the anode, which contains a maximum of six components: the deposited carbon C, CO, H_2, CO_2, H_2O, and CH_4 [42]. As many researchers have reported [41–44], if the operating parameters were finely optimized, especially balancing the supply of methane and the oxygen ion flux (current load), the SOFC system will keep running stably. Apparently, the balance was broken under the conditions in Fig. 7(a), and the carbon deposition process overwhelmed the other reactions. The

excessive accumulation of deposited carbon finally resulted in a crack in the cell.

3.3.2. Stability of the cell operated on pure methane in the RDCFC mode

Fig. 8 shows a typical RDCFC process with six cycles at $J_w = 416$ mA cm^{-2} at 825 °C. The stability test of RDCFC mode was terminated after six cycles, although the cell seemed that more cycles could have been run. Note that the accumulative total power-generation time of the RDCFC test was more than 30 min, which is obviously longer than that in Fig. 7(a). These data suggest that even under the much more favorable conditions for carbon deposition, such as pure methane, $J_w = 0$ and high temperature, controlling the carbon deposition, herein by limiting the duration of carbon deposition to 5 min, still allows the carbon to be utilized as fuel and maintains the fuel cell operating stably in the RDCFC mode.

3.3.3. Stability of the cell operated on pure methane in the intermittent fuel supply mode

Fig. 9(a) shows a typical continuous power-generation process, where the cell operates on 80 ml min^{-1} pure methane by the intermittent fuel supply mode (IFS). As shown in Fig. 9(a), a 5-cycle operation was carried out at $J_w = 416$ mA cm^{-2} at 825 °C. After the operation, the cell's integrity was maintained very well, and there was no obvious carbon deposition on the anode (Fig. 9(b)). Compared with the RDCFC mode, one of the main advantages of the IFS mode is that it is a continuous power-generation process, although the output fluctuates to a certain extent. In addition, the output duration was significantly improved over that in Fig. 8.

The IFS mode could be regarded as a hybrid of the continuous fuel supply mode and the RDCFC mode. In the 5-min pure methane supply stage, the cell was operated at $J_w = 416$ mA cm^{-2}. Obviously, such a high current density can significantly suppress the carbon deposition due to the direct electrochemical oxidation of the solid carbon. On the other hand, the carbon deposition was also suppressed by the reforming reactions of the anode products, steam/CO_2. In the period without supplying methane, the deposited carbon at the anode became the main fuel, although the reforming products of CO, H_2 and some residual methane were present. The cell voltage decreased gradually with the consumption of the solid carbon, and the anode was simultaneously recovered.

Fig. 10(a) shows a six-cycle operation of an SOFC operated under the intermittent methane supply mode at 825 °C. Note that after the first six-cycle operation, a two-step oxidation-and-reduction maintenance process was carried out for the cell: first, the residual carbon was removed from the anode by introducing 20% O_2 in Ar at a 40 ml min^{-1} flow rate in 10 min, and second, the anode was reduced by introducing hydrogen at 40 ml min^{-1} for 30 min (see Fig. 5(b)). After the maintenance process, the second six-cycle operation was performed as shown in Fig. 10(b).

Fig. 10(c) shows the comparison of the normalized relative stability of the four cycling operation cases in this work. The normalized relative stability is obtained by normalizing the power-generation time of the cell using deposited carbon fuel in each cycle period. The relative stability of the second six-cycle operation was obviously higher than that of the first six-cycle operation, supporting the residual carbon hypothesis. The former three cycles of the RDCFC operation were very steady, yet the latter three cycles degraded similar to the five-cycle operation and the first six-cycle operation. In brief, after the maintenance treatment, the stability of the cell operation was improved to a certain extent.

3.4. Polarization effect

Fig. 11 (a)&(d) show the I-V curves of the cells operated under H_2 at 80 ml min^{-1} before and after the RDCFC cycling process (Section 3.3.2) and the 12-cycle process (Section 3.3.3), respectively. The

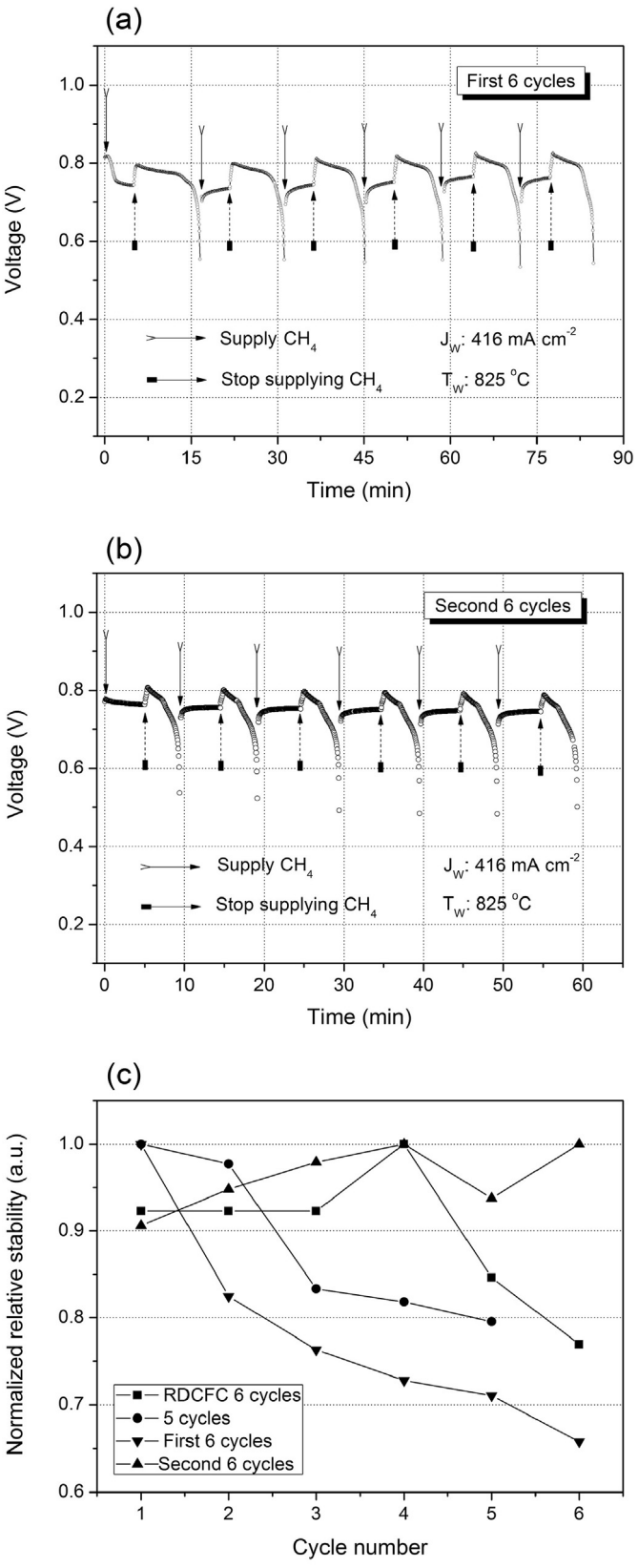

Fig. 10. Voltage versus time of the cell operated at a constant current density of 416 mA cm^{-2} at 825 °C under the intermittent methane supply mode: (a) first 6 cycles, (b) second 6 cycles; (c) the normalized relative stability of the cycling operations.

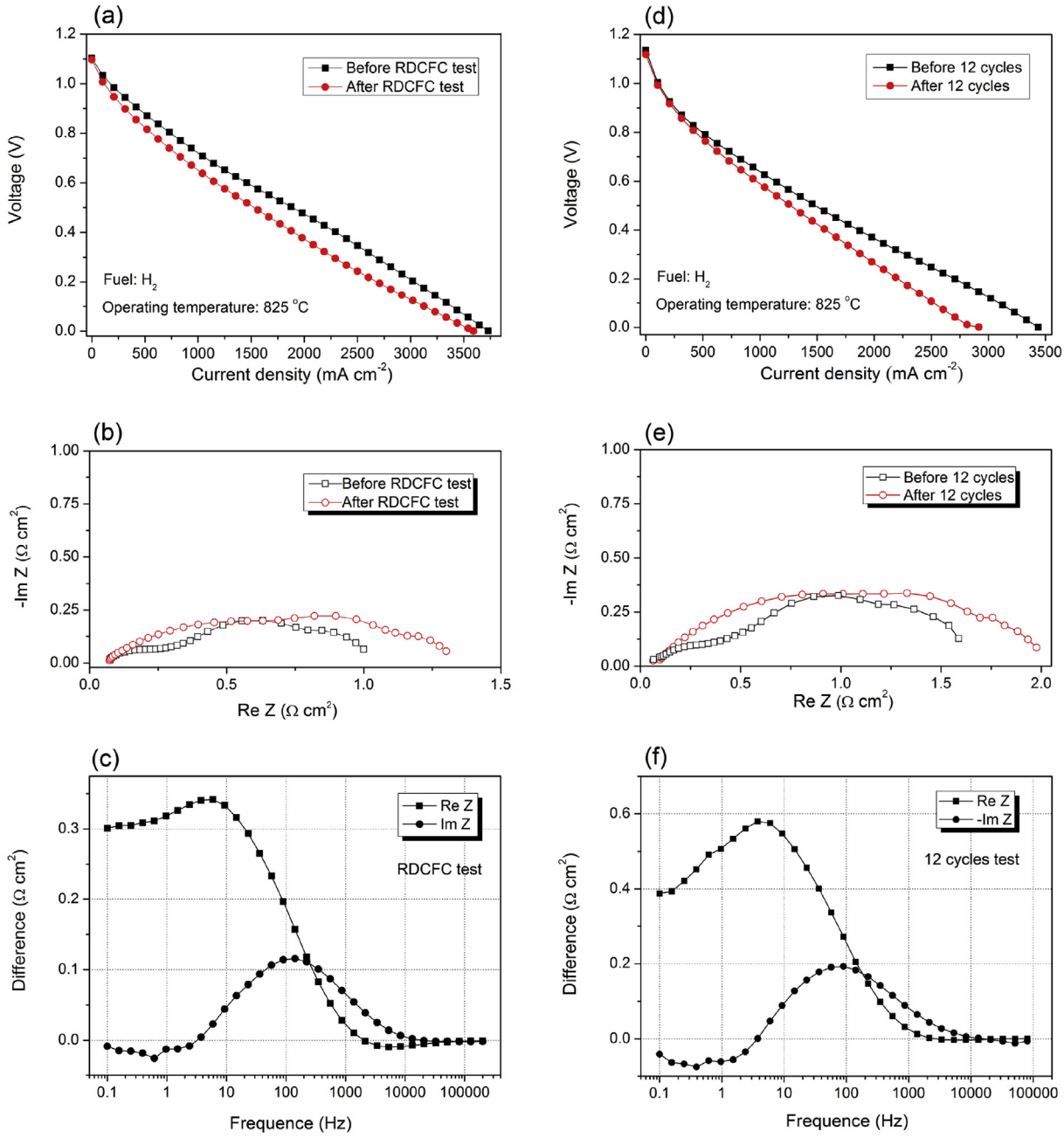

Fig. 11. I-V curves of the cells operated (a) before and after the RDCFC test (Section 3.3.2), and (d) before and after the 12-cycle test (Section 3.3.3). Impedance spectra of the cells operated (b) before and after the RDCFC test, and (e) before and after the 12-cycle test, and the corresponding impedance difference spectra (c) and (f), respectively.

OCV values were almost maintained at 1.1 V before and after the processes, indicating that the electrolyte film was sufficiently dense and that the cell was tightly sealed. However, the performance of the cell obviously degraded to a certain extent after the processes. Fig. 11 (b)&(e) show the AC impedance spectra, and Fig. 11 (c)&(f) give the impedance difference spectra before and after the RDCFC process and the 12-cycle process, respectively.

In general, the low frequency intercept of the impedance arc on the real axis corresponds to the total resistance of the cell, which can be divided into ohmic and electrode polarization resistances [10]. The high frequency intercept represents the ohmic resistance (R_o), involving the ionic resistance of the electrolyte, the electronic resistance of the electrodes, and some contact resistance associated with the interfaces. The difference between the high frequency and low frequency intercepts on the real axis represents the electrode (both anode and cathode) polarization resistance (R_p). Fig. 11 (b)&(e) clearly indicate that after the RDCFC process and the 12-cycle process, the R_p of the cell increased to a certain extent, yet the R_o showed almost no change.

Fig. 11 (c)&(f) show the impedance difference spectra defined as the difference of the resistances (Re Z) or capacitances (Im Z) relative to the corresponding frequency between the values measured before and after a certain process. The impedance difference spectra are featured by a resistance jump phenomenon in approximately 10–1000 Hz and a capacitance peak centered at ~100 Hz. Generally, the high frequency (HF > 10 kHz) response arises from the electrolyte resistance, and the medium and higher frequency (MF, 100-10 kHz) responses are related to the impedance

of the electron-transfer and ion-transfer processes occurring at the current collector/electrode and electrode/electrolyte interfaces, respectively [45]. It has been reported that the response centered at 100–1000 Hz arises from charge-transfer processes, while the response at ~300 Hz was related to an anode electrochemical process [38,40]. The response at the low frequency (LF, 0.1–100 Hz) normally arises from gas diffusion process in porous anodes [38]. Because the frequency range 10–1000 Hz, where the resistance jump phenomenon occurred, belongs to the transition range from LF to MF, the resistance jump phenomenon and the capacitance peak may be associated with the convoluted responses for charge transfer and gas diffusion processes in anodes.

Based on prior observations [39,41], we could presume that the resistance jump phenomenon may originate from the formation of residual carbon and NiO at the anode. As mentioned above, because the carbon deposited on the Ni surfaces has the lowest electrochemical reactivity than those on the TPB and YSZ surfaces, some carbon of this type might become residual carbon that will not be electrochemically oxidized but occupy the Ni active sites [23]. The residual carbon may reduce the pore connectivity and hinder gas diffusing through the porous anode, leading to the increase of anode polarization [39]. On the other hand, a certain quantity of NiO may appear at the anode, which originates from the DCFC process while deposited carbon fuel is being consumed or exhausted. The O^{2-} conducted through the YSZ electrolyte can spill over from the Ni-YSZ interface to the Ni surface (Eq. (11), Fig. 12), and can consequently react with the carbon deposited on the Ni surface through the reactions in Eq.(12)–(17) [23,26]:

$$ {}^{*}O^{2-}_{YSZ} \leftrightarrow {}^{*}O^{2-}_{Ni} \tag{11} $$

$$ {}^{*}C_{Ni} + {}^{*}O^{2-}_{Ni} \leftrightarrow {}^{*}CO^{2-}_{Ni} \tag{12} $$

$$ {}^{*}CO^{2-}_{Ni} \leftrightarrow {}^{*}CO^{-}_{Ni} + e^{-} \tag{13} $$

$$ {}^{*}CO^{-}_{Ni} \leftrightarrow CO_{Ni} + e^{-} \leftrightarrow CO\uparrow \tag{14} $$

$$ CO_{Ni} + {}^{*}O^{2-}_{Ni} \leftrightarrow {}^{*}OCO^{2-}_{Ni} \tag{15} $$

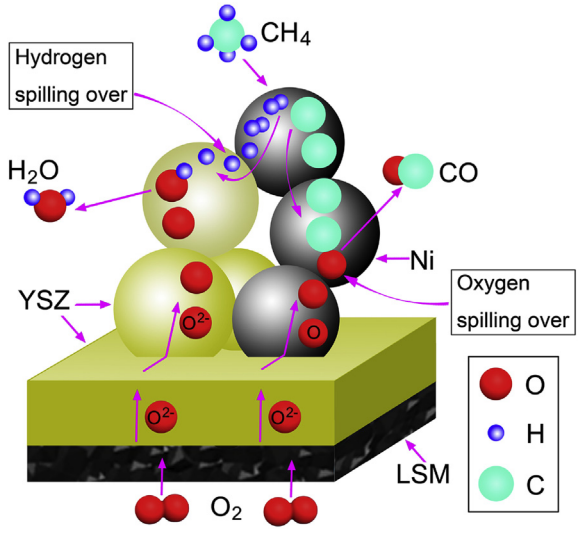

Fig. 12. Schematic illustration of the electrochemical oxidation of hydrogen and deposited carbon on the Ni–YSZ anode.

$$ {}^{*}OCO^{2-}_{Ni} \leftrightarrow {}^{*}OCO^{-}_{Ni} + e^{-} \tag{16} $$

$$ {}^{*}OCO^{-}_{Ni} \leftrightarrow OCO_{Ni} + e^{-} \leftrightarrow CO_2\uparrow \tag{17} $$

When the O^{2-} spilled over to the Ni surface ($^{*}O_{Ni}$) cannot encounter the active carbon at the anode ($^{*}C_{Ni}$), the reactions in Eq. (18) might occur [22,23] and thus the NiO may be formed:

$$ {}^{*}O^{2-}_{Ni} \leftrightarrow {}^{*}NiO^{2-} \leftrightarrow NiO + 2e^{-} \tag{18} $$

The residual carbon and NiO on the anode will be formed and accumulated gradually with the running of the RDCFC or the intermittent fuel supply process, and will result in the decrease of the Ni active sites over the anode. According to the mechanism model of hydrogen oxidation at the anode [46], the hydrogen molecules are first adsorbed and dissociated on the Ni surface (Eq. (19)), then the Ni-adsorbed hydrogen atoms ($^{*}H_{Ni}$) move over the TPB towards the YSZ surface and simultaneously transfer their electrons to the Ni electrode (Eq. (20), Fig. 12). On the YSZ surface, they can attach either to O^{2-} (Eq. (21)) or OH^{-} sites (Eq. (22)).

$$ \uparrow H_2 \leftrightarrow {}^{*}H_{Ni} + {}^{*}H_{Ni} \tag{19} $$

$$ {}^{*}H_{Ni} \leftrightarrow {}^{*}H^{+}_{YSZ} + e^{-} \tag{20} $$

$$ {}^{*}H^{+}_{YSZ} + {}^{*}O^{2-}_{YSZ} \leftrightarrow {}^{*}OH^{-}_{YSZ} \tag{21} $$

$$ {}^{*}H^{+}_{YSZ} + {}^{*}OH^{-}_{YSZ} \leftrightarrow {}^{*}H_2O_{YSZ} \tag{22} $$

$$ {}^{*}H_2O_{YSZ} \leftrightarrow H_2O\uparrow \tag{23} $$

The reactions in Eq. (19) and Eq. (20) are the rate limiting steps of the electrochemical oxidation of H_2, which are closely related with the number of Ni active sites over the anode. The formation of residual carbon and NiO on the anode can reduce the number of Ni active sites and thus inhibit these reactions. The NiO may impede the charge transfer process happened at the Ni particles (Eq. (20)) or TPB at the anode and induce the capacitance peak in the impedance difference spectra. These inhibition/impedance effects will result in the enhanced polarization effect at the anode, in particular, the resistance jump phenomenon in the MF to LF range, as detected by the EIS (see Fig. 11). Note that the amount of NiO is too small to make the R_o increase.

4. Conclusion

The stability of Ni-YSZ anode-supported SOFCs operated on 25% dry methane and on pure methane with three operating modes was investigated at 800 °C and 825 °C, respectively. A successive multi-stage process was performed to explore the operation of cells using 25% dry methane or deposited carbon from methane decomposition as the fuel. Stable operation can be maintained by optimizing the fuel supply and current density parameters. The AC impedance analysis suggests that the partial oxidization of Ni could occur at the anode when carbon fuel was consumed. The cell could run at a comparatively stable state with continuous power output in an intermittent methane supply mode, where the deposition and utilization of carbon was controlled by balancing the fuel supply and consumption. The increase in the polarization resistance of the cell might originate from the small amount of NiO and residual carbon at anodes which can be removed via an oxidation-and-reduction maintenance process. Based on the strategy of controlled carbon deposition and utilization, this work provides an

alternative operating mode for improving the stability of direct methane SOFCs and the feasibility of their application.

Acknowledgments

This work was supported by the National Science Foundation for Distinguished Young Scholars of China (51025209), the Key Technologies R&D Program of Shanxi of China (20150313003-3), the Basic Research Program of Shanxi of China (2015012016), the Program for Innovation Infrastructure Construction of Shanxi of China (2014091019), the Shanxi Scholarship Council of China (2014-015), and the Program for the Selected Sci-tech Activities of Returned Overseas Scholars of Shanxi of China (2014).

References

[1] Energy. In: Penner SS, editor. Assessment of research needs for advanced fuel cells, 11; 1986. l–230.
[2] Appleby AJ. Fuel cell technology: status and future prospects. Energy 1996;21. 521–653.
[3] Lund H. Renewable energy strategies for sustainable development. Energy 2007;32:912–9.
[4] Olabi AG. The 3rd international conference on sustainable energy and environmental protection SEEP 2009, Guest Editor's introduction. Energy 2010;35: 4508–9.
[5] Olabi AG. 100% sustainable energy. Energy 2014;77:1–5.
[6] Gür TM. Comprehensive review of methane conversion in solid oxide fuel cells: prospects for efficient electricity generation from natural gas. Prog Energy Combust Sci 2016;54:1–64.
[7] Wang W, Su C, Wu Y, Ran R, Shao Z. Progress in solid oxide fuel cells with nickel-based anodes operating on methane and related fuels. Chem Rev 2013;113:8104–51.
[8] Rokni M. Thermodynamic analysis of SOFC (solid oxide fuel cell)-stirling hybrid plants using alternative fuels. Energy 2013;61:87–97.
[9] Zhan ZL, Barnett SA. An octane-fueled solid oxide fuel cell. Science 2005;308: 844–7.
[10] Lin YB, Zhan ZL, Liu J, Barnett SA. Direct operation of solid oxide fuel cells with methane fuel. Solid State Ion 2005;176:1827–35.
[11] Xiao J, Xie Y, Liu J, Liu M. Deactivation of nickel-based anode in solid oxide fuel cells operated on carbon-containing fuels. J Power Sources 2014;268:508–16.
[12] Koh JH, Yoo YS, Park JW, Lim HC. Carbon deposition and cell performance of Ni-YSZ anode support SOFC with methane fuel. Solid State Ion 2002;149: 157–66.
[13] Murray EP, Tsai T, Barnett SA. A direct-methane fuel cell with a ceria-based anode. Nature 1999;400:649–51.
[14] Shao Z, Haile SM, Ahn J, Ronney PD, Zhan Z, Barnett SA. A thermally self-sustained micro solid-oxide fuel-cell stack with high power density. Nature 2005;435:795–8.
[15] Li K, Jia L, Wang X, Pu J, Chi B, Li J. Methane on-cell reforming in nickel–iron alloy supported solid oxide fuel cells. J Power Sources 2015;284:446–51.
[16] Sariboğa V, Öksüzömer F. The investigation of active Ni/YSZ interlayer for Cu-based direct-methane solid oxide fuel cells. Appl Energy 2012;93:707–21.
[17] Choi S, Sengodan S, Park S, Ju Y-W, Kim J, Hyodo J, et al. A robust symmetrical electrode with layered perovskite structure for direct hydrocarbon solid oxide fuel cells: $PrBa_{0.8}Ca_{0.2}Mn_2O_{5+d}$. J Mater Chem A 2016;4:1747–53.
[18] Yang F, Gu J, Ye L, Zhang Z, Rao G, Liang Y, et al. Justifying the significance of Knudsen diffusion in solid oxide fuel cells. Energy 2016;95:242–6.
[19] Jia J, Li Q, Luo M, Wei L, Abudul A. Effects of gas recycle on performance of solid oxide fuel cell power systems. Energy 2011;36:1068–75.
[20] Alzate-Restrepo V, Hill JM. Effect of anodic polarization on carbon deposition on Ni/YSZ anodes exposed to methane. Appl Catal A Gen 2008;342:49–55.
[21] Liu J, Barnett SA. Operation of anode-supported solid oxide fuel cells on methane and natural gas. Solid State Ion 2003;158:11–6.
[22] Gür TM. Critical review of carbon conversion in “carbon fuel cells”. Chem Rev 2013;113:6179–206.
[23] Li C, Shi Y, Cai N. Mechanism for carbon direct electrochemical reactions in a solid oxide electrolyte direct carbon fuel cell. J Power Sources 2011;196: 754–63.
[24] Li C, Shi Y, Cai N. Effect of contact type between anode and carbonaceous fuels on direct carbon fuel cell reaction characteristics. J Power Sources 2011;196: 4588–93.
[25] Giddey S, Badwal SPS, Kulkarni A, Munnings C. A comprehensive review of direct carbon fuel cell technology. Prog Energy Combust Sci 2012;38:360–99.
[26] Horita T, Yamaji K, Kato T, Kishimoto H, Xiong YP, Sakai N, et al. Imaging of CH_4 decomposition around the Ni/YSZ interfaces under anodic polarization. J Power Sources 2005;145:133–8.
[27] Vayenas CG, Bebelis S, Neophytides S, Yentekakis IV. Non-faradaic electrochemical modification of catalytic activity in solid electrolyte cells. Appl Phys A Mater Sci Process 1989;49:95–103.
[28] Ihara M, Matsuda K, Sato H, Yokoyama C. Solid state fuel storage and utilization through reversible carbon deposition on an SOFC anode. Solid State Ion 2004;175:51–4.
[29] Ihara M, Hasegawa S. Quickly rechargeable direct carbon solid oxide fuel cell with propane for recharging. J Electrochem Soc 2006;153:A1544–6.
[30] Hasegawa S, Ihara M. Reaction mechanism of solid carbon fuel in rechargeable direct carbon SOFCs with methane for charging. J Electrochem Soc 2008;155: B58–63.
[31] Saito H, Hasegawa S, Ihara M. Effective anode thickness in rechargeable direct carbon fuel cells using fuel charged by methane. J Electrochem Soc 2008;155: B443–7.
[32] Jiao Y, Tian W, Chen H, Shi H, Yang B, Li C, et al. In situ catalyzed boudouard reaction of coal char for solid oxide-based carbon fuel cells with improved performance. Appl Energy 2015;141:200–8.
[33] Shao Z, Zhou W, Zhu Z. Advanced synthesis of materials for intermediate-temperature solid oxide fuel cells. Prog Mater Sci 2012;57:804–74.
[34] Larminie J, Dicks A. Fuel cell systems explained. second ed. Chichester, West Sussex, England: John Wiley & Sons Ltd.; 2003.
[35] EG&G Services, Inc. Fuel cells: a handbook. seventh ed. Morgantown, West Virginia: US Department of Energy; 2004.
[36] Chen G, Wang Y, Sunarso J, Liang F, Wang H. A new scandium and niobium co-doped cobalt-free perovskite cathode for intermediate-temperature solid oxide fuel cells. Energy 2016;95:137–43.
[37] Primdahl S, Mogensen M. Gas conversion impedance: a test geometry effect in characterization of solid oxide fuel cell anodes. J Electrochem Soc 1998;145: 2431–8.
[38] Kennouche D, Chen-Wiegart YCK, Riscoe C, Wang J, Barnett SA. Combined electrochemical and X-ray tomography study of the high temperature evolution of Nickel-Yttria Stabilized Zirconia solid oxide fuel cell anodes. J Power Sources 2016;307:604–12.
[39] Ding J, Liu J, Yin G. Cell/stack electrochemical performance and stability of cone-shaped tubular SOFCs for direct operation with methane. Electrochim Acta 2011;56:6593–7.
[40] Kennouche D, Chen-Wiegart YCK, Cronin JS, Wang J, Barnett SA. Three-dimensional microstructural evolution of Ni-yttria-stabilized zirconia solid oxide fuel cell anodes at elevated temperatures. J Electrochem Soc 2013;160: F1293–304.
[41] Chen G, Guan G, Abliz S, Kasai Y, Abudula A. Rapid degradation mechanism of Ni-CGO anode in low concentrations of H_2 at a high current density. Int J Hydrogen Energy 2011;36:8461–7.
[42] You HX, Gao HJ, Chen G, Abudula A, Ding XW. The conversion among reactions at Ni-based anodes in solid oxide fuel cells with low concentrations of dry methane. J Power Sources 2011;196:2779–84.
[43] Pillai M, Lin YB, Zhu HY, Kee RJ, Barnett SA. Stability and coking of direct-methane solid oxide fuel cells: effect of CO_2 and air additions. J Power Sources 2010;195:271–9.
[44] Bunin GA, Wuillemin Z, François G, Nakajo A, Tsikonis L, Bonvin D. Experimental real-time optimization of a solid oxide fuel cell stack via constraint adaptation. Energy 2012;39:54–62.
[45] Adler SB. Factors governing oxygen reduction in solid oxide fuel cell cathodes. Chem Rev 2004;104:4791–843.
[46] Shishkin M, Ziegler T. Hydrogen oxidation at the Ni/yttria stabilized zirconia interface: a study based on density functional theory. J Phys Chem C 2010;114:11209–14.